https://doi.org/10.5194/egusphere-2023-425
Preprint. Discussion started: 18 April 2023

Probabilistic Methods for Projecting Average Recurrence Intervals of Coastal Flooding with Sea Level Rise

Timothy M. Hall[1], James P. Kossin[1], Terence Thompson[1], Seung H. Baek[1], Kimberly L. Drouin[1], Danielle Montagne[1]

[1]The Climate Service, an S&P Global Company

Correspondence to: Timothy Hall (timothy.hall@spglobal.com)

Abstract. We illustrate efficient methods to estimate future projected average return intervals (ARIs) of flood depths in coastal regions from storm-tide data and sea-level rise (SLR) projections. A flood-water path-finding algorithm is applied to digital elevation models (DEMs) in coastal regions to determine possible flood depths at interior points, given storm-tide levels at ARIs and local SLR with uncertainty on the coast. We show that the distribution of projected ARIs of a historical baseline flood-depth is truncated log-normal in the Gumbel extreme-value approximation, and we provide analytic expressions for the means. With this approximation, projected change in flood damage over a range of ARIs can be estimated by analysis at any single ARI. Compared to flood-depth distributions, ARI distributions are less directly related to flood damage, but they have the advantage of relative insensitivity to uncertainties in DEMs and other granular details of flood-risk modeling. We illustrate with applications to Miami, Florida, and coastal North Carolina using two different DEMs.

1 Introduction

Sea-level rise (SLR) exacerbates flooding due to coastal storm surge and tides (collectively termed storm tides) by increasing the background water level on top of which the storm tide propagates. Research in projecting future storm tide levels with SLR is extremely active (e.g., Lin et al, 2016; Vitousek et al., 2017; Vousdoukas et al, 2018; Muis et al, 2016; 2020; Kirezci et al., 2020; Sweet et al., 2022), and calculating coastal flood loss in response to storm tide and SLR is a crucial component of climate-risk analysis. Estimation of damage to infrastructure and buildings traditionally involves granular representation of the affected structures, such as baseboard elevation, construction components, and flood proofing measures (Scawthorn, et al., 2006), as well as insurance loss data for validation (Wing et al, 2020). The physical modeling requires accurate elevation data at resolutions of a few 10s of meters or better, along with detailed modeling of the hydraulics and the meteorological drivers (e.g., Bates et al., 2021). Such a granular representation, however, is not always practical when providing decades-long projections of climate-related hazards and risks due to numerous perils on a global scale.

An alternative approach is to consider the change in the average recurrence interval (ARI) of a specified historical-baseline flood depth as a function of SLR projections. Examples include the New York City analysis of Lin et al. (2016) addressing Hurricane Sandy surge under SLR scenarios and the US-coastal analysis of Taherkhani et al. (2020) illustrating the exponential sensitivity of return period to SLR. (ARI is closely related to return period, as discussed

https://doi.org/10.5194/egusphere-2023-425
Preprint. Discussion started: 18 April 2023

below.) In such an approach, the flood-depth itself is not explicitly provided, and the calculation of the change in flood ARI due to SLR is effectively separated from the calculation of the absolute baseline flood hazard. Estimation of the change, which is primarily driven by the lower-resolution envelope of SLR, requires less granular representation than the absolute flood hazard and risk. While the granular baseline modeling is necessary for accurate projections of loss to structures, the less-granular ARI analysis captures the change from that baseline. For example, the baseline 100-yr flood could be 0.1m or 1.0m; in either case, in certain limits discussed here, a SLR of 0.5m results in approximately the same projected ARI of that baseline 100-yr event. If the baseline loss is known independently, e.g., from detailed engineering studies, then this loss can be combined with the change estimate to project absolute risk.

We take this ARI approach at The Climate Service (TCS), an S&P Global company providing decadal climate risk projections globally for a range of climate and weather hazards. We use storm tide levels provided at highly-resolved global coastal locations and a range of ARIs, as computed by the Global Tide and Surge Reanalysis (GTSR) hydrodynamic model driven by reanalysis wind fields (Muis et al., 2016). Known biases in the GTSR storm tides in regions with tropical cyclone activity are reduced using observational tide-gauge analysis (Zervas, 2013). We combine the storm tides and regional projections of SLR with uncertainty from Kopp et al (2014) to obtain projected storm tide estimates at a range of ARIs. Resulting flood depths at interior points from the coast are estimated using a modified bathtub approach that represents hydrological connectivity according to elevation data from (i), a 1 arc-second (~30m) digital elevation model (DEM) for the contiguous US and (ii), a 3 arc-second (~90m) DEM for global regions outside CONUS. To represent hydrological connectivity, we compute at each elevation "pixel" in our coastal domains (1 arc-second or 3 arc-second) the minimum elevation threshold (MET) that nearby coastal waters would need to attain in order to inundate the pixel, as discussed below. Finally, the flood depths are used to calculate projected ARIs corresponding to historical baseline depths.

Our approach does not consider the dynamical nature of storm-flooding events, which feature finite duration, flood propagation rates and inland penetration, as well as waves. While coastal storm events drive the GTSR modeling, once the storm-tide data is obtained in ARI form from Muis et al (2016), events are no longer explicitly represented. This reduces the realism of modeled flood depths, but it has the advantage of allowing us to represent the flood resulting from a range of events without modeling the events explicitly. In fact, the same MET analysis can be applied to steady secular SLR inundation, independent of storm tide. In addition, as discussed below, the use of ARI rather than depth limits the sensitivity to missing physical elements of the modeling, as well as uncertainties in the DEMs.

A robust feature of our ARI approach is that, to the extent the baseline storm-tide distribution is approximately Gumbel, the change in the mean flood loss to a structure over all ARIs can be determined by the change at a single ARI. Thus, with the Gumbel assumption, only the 100-yr ARI flood loss (nearly identical to the 100-yr return-period flood loss, as discussed below) need be considered to estimate the change at any ARI, or averaged over all ARIs. In addition, we present a probabilistic framework for the ARI approach that encompasses the large uncertainty in SLR projections. Within the Gumbel limit, ARI projections are distributed log-normally, with truncations as dictated by

https://doi.org/10.5194/egusphere-2023-425
Preprint. Discussion started: 18 April 2023

elevation considerations. Expressions are derived for the truncations and the means of the truncated distributions. Use of these relationships greatly reduce computational expense in determining spatial flood-ARI maps over global coastal regions at high resolution.

The paper is organized as follows: Section 2 discusses the spatial domains, elevation fields, and coastline data; while Section 3 presents the path-finding analysis to calculate flood depths at interior locations. In Section 4, we discuss the historical reference-period coastal storm tide estimates and their debiasing in active tropical cyclone regions. Our probabilistic analysis of ARIs is presented in Section 5. We illustrate with examples in Section 6, and summarize and conclude in Section 7.

2 Coastal Domains and DEMs

Our coastal analysis spans the global continental coastline and near-continental islands, as approximately 4000 additional remote islands (Fig 1). For CONUS, we use the 1-arc-second resolution (~30m at the equator) DEM provided by the US Geologic Survey referred to as 3DEP (Stoker and Miller, 2022). 3DEP estimates ground elevation using lidar and other data sources and is one of the most accurate publicly available uniform elevation fields over CONUS. Importantly, 3DEP removes approximately the influence of tree canopies and buildings on ground elevation estimates. The 3DEP DEM is provided in 1°-by-1° "tiles" of dimension 3600-by-3600 "pixels." Each pixel is rectangular in longitude and latitude, with sides of 1 arc-second. For the remaining global coastline, we use the MERIT DEM (Yamazaki et al., 2017), which has a resolution of 3 arc-seconds (~90m at the equator). MERIT is a signal-processed analysis of SRTM satellite data that removes unrealistic features in SRTM and corrects for tree canopies (Yamazaki et al., 2017). Unlike in 3DEP, no specific effort was made in MERIT to remove buildings (McClean et al., 2020); buildings can therefore cause positive bias when using MERIT to approximate ground elevation, to the extent they are not resolved at 3 arc-seconds. MERIT is provided in 5°-by-5° tiles, each of dimension 6000-by-6000 pixels.

As part of the calculations described below, we employ 30m-resolution global (continents and islands) coastline data from USGS (Sayre et al., 2019). These data are provided in six continental units (North America, South America, Eurasia, Asia-East, Africa, and Australia) and separate individual island units. At present we use the 3760 largest explicitly-named islands, which includes islands as small as 1 to 2 km in scale. We note that many additional islands are also analyzed implicitly; if an island is close enough to a continental coastline or another explicitly-named island, it will sit inside the analysis boxes for the path-finding calculations along the continental or named-island coastline, as discussed below.

3 Path-Finding Algorithm and the Minimum Elevation Threshold

Whether a location that is interior from the coast is flooded in response to a specified coastal water level depends not only on the site's elevation, but also on intervening elevation. A location may be lower than the coastal water level but be protected from flooding by a natural or artificial intervening barrier that is higher than the coastal water level.

https://doi.org/10.5194/egusphere-2023-425
Preprint. Discussion started: 18 April 2023

Therefore, determining whether a location can be flooded requires analysis of elevation along a multiplicity of paths that connect the coast to the site. This consideration of intervening elevation distinguishes our approach from a "bathtub" model, in which only the site's elevation is considered.

We use the elevation data summarized above to compute gridded spatial maps of the minimum elevation threshold (MET). The MET at a location is the minimum water level required at the nearby coast to inundate the location. That is, among the various paths to the location from the coast, the MET is the minimum value in the set of highest elevations along paths from the coast to the location. If a storm tide at the coast has water level h_{ST}, and there is a path to the location that is lower everywhere than the location's elevation, h_{EL}, then the MET simply equals h_{EL}. However, if every path to the location has somewhere an elevation greater than h_{EL}, then the MET is the lowest of the maximum elevations along the paths. This MET is the storm tide level that could, in principle, just inundate the site by taking the least elevated path.

The map of METs is computed using a Dijkstra algorithm, as described by Grady and Xingong (2018). The algorithm is initialized on a set of coastal pixels. The MET values on these initial pixels are set equal to the elevation of the pixels, and the initial pixels are marked as "visited." The pixel in this set with the minimum elevation is located. The algorithm then moves on to the unvisited pixels adjacent (eight sides and corners) to this minimum-elevation pixel and finds the minimum among this new set. If the new minimum has a higher elevation than any of its previously visited neighbors, then its MET is assigned that elevation. If its elevation is lower than the minimum elevation of its previously visited neighbors, then its MET is the previous minimum. The procedure is iterated until all pixels in the domain are visited.

The spatial domain for the MET fields and the initial set of coastal pixels has to be specified. Computational expense prevents the calculation of METs over the full DEM tiles. In addition, it is desireable to specify initial fronts small enough to resolve the GTSR storm-tide variation along the coast. We choose overlapping rectangular MET domains ("boxes") of sides 0.25° centered on USGS coastline vertices, with box centers separated along the USGS coastal contour by 12.5km (Fig 2). Within a box, the initial front is defined as the set of coastal pixels that are closer to that box's center than to any other box center. The storm tide assigned uniformly to the points on the initial front is the GTSR storm tide (one value for each of the nine GTSR ARIs) at the GTSR coastal point closest to the MET box center. Subsequently, the GTSR storm tide is incremented with SLR values from the SLR coastal tide-gauge station location (Kopp et al, 2014) that is closest to the selected GTSR point.

The overlap in the MET boxes means that a given interior location will in general have more than one MET value assigned to its pixel. For example, if the pixel lies within four overlapping boxes, then it will have four METs, one with respect to each of the boxes' distinct set of coastal initial-front pixels (Fig 3). This is because the flow paths to the interior pixel from the four sets of coastal pixels are different, with different elevations along the paths. To assign a single MET to the interior pixel from among the multiple METs, we choose the MET that has lowest value h_{MET}

https://doi.org/10.5194/egusphere-2023-425
Preprint. Discussion started: 18 April 2023

compared to the GTSR 100-year storm-tide h_{ST} associated with its set of coastal pixels, i.e., the MET with the minimum value of h_{ST} - h_{MET}. Physically, this is the MET that would most easily allow flooding. This accounts for both variations in path elevations from different coastal location and variations in storm-tides on those coastal locations.

The selections of MET box size 0.25° and spacing 12.5km are compromises between computational expense and resolution of storm tide and path variations. Ideally, large boxes would be specified, encompassing interior locations far from the coast that might in principle be reached by coastal storm tides, especially in low-lying regions. However, the Dijkstra path-finding algorithm computational cost increases with the number of pixels in the box. This cost and the need for global coverage limits the box size. In partial justification of the 0.25° box size, we note that storm surge and tide are dynamical events with a typical timescale of less than one day and that flood-water propagation rates are finite. Coastal waters rise and propagate inland, then subsequently fall and retreat back to the coast. It is rare for storm tide flood waters to penetrate more than roughly 10km inland. The choice of 0.25° box size (~25km, typically reaching 10-15km inland) accommodates most of this penetration. In addition, the high-resolution USGS coastline follows most major and many minor rivers and estuaries that can carry storm waters for many kilometers inland.

As for the spacing between adjacent boxes, the closer the boxes, the smaller are the set of initial-front pixels, and the better resolved is the geographic structure in storm tide and SLR. The SLR, however, has little geographic variation at the scale of our selected 12.5km box spacing. By contrast, storm tides can have geographic variation on this scale via surge and tide amplification in bays and estuaries. The GTSR ARI storm tide levels are provided at points along the coastline with varying separations, and about 40% of these separations are less than 12.5km. However, the average difference in the 100-yr GTSR storm-tide magnitude between adjacent points separated less than 12.5km is only 0.01m. Even for adjacent points separated in the range 10km to 12.5km, the average 100-year storm-tide adjacent-point difference is only 0.04m. By comparison, the average 100-year storm-tide difference for separations greater than 12.5km is 0.28m. Given other approximations and sources of error in the analysis, as well as known biases in the GTSR storm-tides (see below), resolution of GTSR storm-tide levels to better than a few centimeters is not warranted, and the choice of 12.5km for MET-box separation is satisfactory.

An example of a MET map is shown in Fig 4. The MET has the effect of smoothing the elevation field, removing local minima in elevation. A local minimum in elevation is protected by the surrounding more elevated environment, and the MET will be assigned a value from that more elevated environment.

4 Storm Tide Debiasing in Active Tropical Cyclones Regions

As indicated above, for storm tide along the global coastline, we make use of values calculated by Muis et al. (2016) using the global hydrodynamic ocean Global Tide and Surge Model (GTSM) driven by 1979-2014 ERA-Interim atmospheric meteorological reanalysis data. The resulting GTSR data comprises 36 years of water level along a highly-resolved coastline. Muis et al (2016) apply Gumbel generalized extreme value (GEV) fits to the annual water-level

https://doi.org/10.5194/egusphere-2023-425
Preprint. Discussion started: 18 April 2023

maxima to estimate storm tide levels at nine return periods: 2, 5, 10, 25, 50, 100, 250, 500, and 1000 years. Distinct storm tide values are provided at a set of 12,145 global coastal locations that vary in separation distance. About 25% of the locations are closer than 5.0km to an adjacent location, while about 25% are further than 50.0km from an adjacent location, typically at high latitudes. There is considerable spatial variation in the storm tide values, driven by factors such as storm climatology, coastline geometry, bathymetry, and tidal amplitude. The minimum 100-yr storm tide is 0.15m (36.86°E, 41.35°N), and the maximum is 8.97m (122.22°E, 4.49°S). Muis et al (2016) also provide coastal points linearly interpolated to less than 1km between locations. When assigning storm tide values to the MET-box initial fronts described above, we use the values of the GTSR interpolated point closest to the MET-box center.

Due primarily to the 0.75° spatial resolution of the ERA-Interim reanalysis wind fields, tropical cyclones (TCs) are not well represented in GTSR. Consequently, the GTSR storm tides are known to be biased low in active TC regions (Muis et al., 2016). In our analysis, we have applied a scheme to reduce this bias that makes use of observationally-based estimates of storm tides from tide-gauge data and maps of global TC activity. Zervas (2013) applied GEV analysis to water-level measurement time series from 82 NOAA tide-gauge stations on the coastal U.S., including Alaska and Hawaii, resulting in estimates of 10-year and 100-year return-period storm-tide levels for these sites. Fig 5 shows scatter plots of the NOAA tide-gauge storm tides and the GTSR storm tides at the same locations. In active TC regions, there is a tendency for the GTSR values to be lower than the tide-gauge estimates.

To reduce the bias, we perform a bivariate linear regression across the 82 tide-gauge sites using the Zervas (2013) storm tides and a measure of local TC activity as the independent variables and the GTSR storm tides as the dependent variable. The regression is performed separately for 100-year and 10-year return-period values. Once the regressions are performed, we can apply the regression coefficients to GTSR storm tides and TC activity measures at locations for which we do not have tide-gauge data, resulting in modified GTSR values that better account for TCs.

In summary, the regression model is

$$y = a_0 + a_1 x_1 + a_2 x_2, \quad (1)$$

where x_1 is the GTSR 100-yr or 10-yr level, x_2 is the gridded kernel-smoothed IBTrACS TC annual occurrence rate (Levinson et al., 2010) for TCs of tropical storm-force and higher. (TC gridding is 0.5° latitude-longitude and the Gaussian kernel bandwidth is 100km.) The OLS coefficient values are $a_0 = 0.47^{0.83}_{0.16}$, $a_1 = 0.84^{0.97}_{0.67}$, and $a_2 = 0.37^{0.62}_{0.16}$, with 5%-95% confidence bands (subscripts and superscripts) determined by a bootstrap resampling of the 82 NOAA tide-gauge sites. The standard deviation of the regression residuals is 0.49m. The sign of the a_2 coefficient is significantly positive, confirming our expectation that TCs have a significant impact on improving the GTSR storm-tide estimates. An illustration of the impact of the debiasing procedure is shown in Fig. 6, along with the global TC rate map.

https://doi.org/10.5194/egusphere-2023-425
Preprint. Discussion started: 18 April 2023

5 Computing Flood-Depth Average Recurrence Intervals and Frequencies

The sections above have described how the METs and storm-tides are determined for a pixel. In this section, we present the methods for computing projected flood-depth and ARI distributions from the METs, storm-tides, and SLR. The flood depth and ARIs are computed as probability density functions (PDFs), driven by the uncertainty distribution in SLR.

5.1 Mean Loss Over Range of ARIs

We motivate the development by discussing calculations of flood damage and financial loss to a hypothetical structure in terms of ARIs, as these are our ultimate applications of the coastal flood analysis. First, we compute the fractional loss to the structure using an idealized function relating fractional loss to flood depth. We then compute the mean fractional loss over all ARIs and show that, within certain limits, the fractional change in the mean loss is a single multiplicative factor, independent of ARI. This independence result is readily generalized to more complicated loss functions.

Consider a fractional loss function L of flood depth, d, with zero mean loss below a threshold, d_0, an intermediate regime of linear increase, and saturation at complete loss above another threshold, d_1.

$$L(d) = \begin{cases} 0, & d \le d_0 \\ \frac{d-d_0}{d_1-d_0}, & d_0 \le d < d_1 \\ 1, & d \ge d_1 \end{cases} \quad (2)$$

The function is illustrated in Fig 7. More complicated loss functions can be accommodated without changing the conclusions, as noted below.

To reframe the analysis in terms of ARI, we make the following key approximation: the relationship between flood depth and ARI is log-linear in the ARI. Approximate log-linear behavior is seen in numerical simulations of storm tides in the ARI range 1-1000 years in the New York region (Lin et al, 2016), while Marsooli et al. (2019) show regional deviation from log-linearity above 100 years. In our case, exact log-linearity in ARI arises from the use of the Gumbel distribution by Muis et al (2016; 2020) to model annual maximum time series of water levels in the GTSR storm-tide model. Gumbel is the class of General Extreme Value (GEV) distributions of maximum values that has a shape parameter of zero, and has been widely used to model sea-level extremes (e.g., Hunter, 2012). Using the Gumbel distribution, depth is $d = \beta \ln(T) + \mu$, where b and m are the Gumbel scale and location parameters respectively, and T is the ARI (see Appendix). More generally, for non-zero shape parameter the log-linearity is violated.

https://doi.org/10.5194/egusphere-2023-425
Preprint. Discussion started: 18 April 2023

GEV shape parameters are notoriously difficult to estimate (Papalexiou and Koutsoyiannis, 2013). This is especially true for data records short compared to the ARIs of events of interest, such as the 36-year GTSR storm-tide series fit by Muis et al. (2016). Regional deviations from log-linearity occur in both directions (Wahl et al., 2017; Marsooli et al., 2019), depending on the sign of the shape parameter. For example, Zervas (2013) obtained positive shape parameters on some regions and negative on others when fitting GEV to US tide-gauge station data, but in the majority of locations the stated uncertainty bands include zero (Gumbel). Vitousek et al (2017) found a global range of shape parameters from -0.18 to +0.20. Wahl et al (2017) concluded that in most global coastal regions the use of Gumbel tends to overestimate long ARI storm-tides. In these regions, the best-fit shape parameters are negative (Weibull distribution), and storm tide is bounded at high ARI. However, in regions with TC activity the shape parameter is positive (Frechet distribution). Taherkhani et al. (2020) fitted GEV to US coastal station data and argued that the zero shape-parameter limit of pure exponential behavior offers important insight to flood-frequency growth rates.

Thus, while the assumption of Gumbel involves error, the sign of the long-ARI error is not uniform, and the simplicity of Gumbel log-linear behavior offers key advantages. In any case, our analysis is weighted towards shorter ARIs, as we estimate the projected shift in the baseline 100-yr flood level under SLR, which is a shift to lower ARI. We are less sensitive to Gumbel limitations at ARIs greater than 100 years.

An important point discussed in the Appendix concerns the use of ARI rather than return period. The ARI definition is distinct from the return period. The ARI, T_{ARI}, of a depth d is the average time between events with depth exceeding d, and the reciprocal of T_{ARI} is the frequency of exceeding d. By contrast, the return period, T_{RP}, is the average time between years having at least one event exceeding d, and the reciprocal of T_{RP} is the annual exceedance probability of exceeding d. In the long ARI or return period limit, $T_{ARI} \sim T_{RP}$. For short return period they differ, which is clear from the fact that T_{RP} is restricted to be greater than one, because probability is always less than one, while T_{ARI} can take any positive value. In the following development, for brevity we use the symbol T for ARI.

Exploiting the log-linearity of d with T, $L(d)$ in equation (2) can be expressed as $L(T)$:

$$L(T) = \begin{cases} \frac{\ln(T)-\ln(T_0)}{\ln(T_1)-\ln(T_0)}, & T_0 \le T \le T_1 \\ 0, & T < T_0 \text{ or } T > T_1. \end{cases} \quad (3)$$

Here, T_0 is the ARI that corresponds to flood depth d_0 in the baseline period, and T_1 corresponds to d_1. The values T_0 and T_1 will generally differ substantially, e.g., T_0 = 2yr (nuisance flooding) and T_1 = 1000yr (total loss). Note that T_0 and T_1 are useful scaffolding for the derivation of mean loss below. In the end, however, the specific values of T_0 and T_1 drop out of the estimation of the fractional projected change in mean loss, which is our goal.

The mean loss, $\bar{L}$, is obtained by summing the incremental losses δL by ARI over all ARIs, weighted by the probability $p(T)$ for an event with ARI T.

https://doi.org/10.5194/egusphere-2023-425
Preprint. Discussion started: 18 April 2023

$$\bar{L} = \sum_T \delta L(T) p(T) \sim \int_{T_0}^{T_1} \frac{dL}{dT} p(T) dT \quad (4)$$

The annual probability is $p(T) = 1/T$ for large T, and we have from above that $\frac{dL}{dT} = k/T$ where $k = (\ln(T_1) - \ln(T_0))^{-1}$. Substituting in (6) and integrating yields

$$\bar{L} = k\left(\frac{1}{T_0} - \frac{1}{T_1}\right) = k(f_0 - f_1) \quad (5)$$

where f is annual event frequency $f = 1/T$.

Equation (5) for $\bar{L}$ was derived for a fixed sea level. In the presence of local projected SLR, the return periods T_0 and T_1, corresponding to the fixed depths d_0 and d_1, are reduced. Because depth is log-linear in ARI, T_0 and T_1 are reduced by an identical fraction, F. Similarly, the frequencies are increased by that fraction, F. In other words, we have

$$\bar{L}(\text{projected}) = F\,\bar{L}(\text{baseline}), \quad (6)$$

where F is independent of ARI T and frequency f. To estimate the projected fractional change, F, in loss, we exploit this independence by considering the change in a single ARI and applying it to other ARIs. The 100-yr reference is a practical choice, because of the extensive literature referencing this ARI.

Equation (6) was derived for a linear variation in $L(d)$ from d_0 to d_1, or equivalently, a linear variation in $L(T)$ from $\ln(T_0)$ to $\ln(T_1)$. This is readily generalized. The linear increasing regions can be replaced by piecewise linear sections, d_0-d_1, d_1-d_2, …, d_{n-1}-d_n, and similarly for T_0-T_1. The same arguments hold, leading to equation (5) for each piecewise segment, and the mean loss over all segments is the sum of the mean losses over the individual segments. For projections, the argument that $\bar{L}$(projected) = F $\bar{L}$(baseline), applies now for the loss on each section, and therefore applies also to the sum of section losses.

5.2 Probability Density Functions for Flood Depth and Frequency

Projections of SLR are uncertain, and it is of considerable interest to propagate this uncertainty to coastal flood and loss projections in order to make projections at low-probability, high-loss percentiles. Kopp et al. (2014) have combined many sources of uncertainty in their SLR projections and provide SLR projections at a range of percentiles and decades under different climate scenarios. The resulting SLR distributions are normally distributed to a close approximation . The uncertainty distribution of storm tides for the projected 100-yr level is the baseline 100-yr level plus the SLR distribution. (We neglect non-linear interactions, for example between tidal amplitude and water depth.)

https://doi.org/10.5194/egusphere-2023-425
Preprint. Discussion started: 18 April 2023

At some location interior from the coast, we assume at first that all flood depths in the distribution driven by the SLR uncertainty can be realized. (This will be relaxed shortly, and the distributions will be truncated to prohibit flood depths that cannot be realized due to elevation, such as negative depths or positive depths lower than flood barriers.) This "unconditional" mean flood depth, a depth computed without consideration of conditions due to topography, is simply

$$\mu_d = d_{ref} + \mu_{SLR} = h_{ST,ref} - h_{EL} + \mu_{SLR}, \quad (7)$$

where d_{ref} is the flood depth of the baseline reference ARI, e.g., d_{100} for the 100-yr ARI, $h_{ST,ref}$ is the corresponding reference ARI storm tide, and h_{EL} is the elevation of the interior location, and μ_{SLR} is the mean local SLR.

Our goal is to estimate the future projected ARI that corresponds to d_{ref}, which in this analysis is d_{100}. Thus, we want to determine the distribution of projected $\ln(T)$ values that correspond to the baseline 100-yr depth, d_{100}. We motivate the relationship graphically. Fig. 8 illustrates the relationship between flood depth, ARI, and projected SLR. Because of the depth-ARI log-linearity, the normal distribution in flood depth on the vertical axis—d_{ref} plus the normal SLR distribution—translates to a normal distribution in $\ln(T)$ on the horizontal axis, which is equivalent by definition to a log-normal distribution in T. The mean and standard deviation of the $\ln(T)$ distribution, $\mu_{ln(T)}$ and $\sigma_{ln(T)}$, can be determined geometrically in Fig. 8 from the mean and standard deviation of the SLR distribution, μ_{SLR} and σ_{SLR}. Using the fact that the slope of the curves, $\tan(\theta)$ in Fig. 8, is the Gumbel scale parameter, β, (Appendix), we have

$$\mu_{\ln(T)} = \ln(T_{ref}) - \frac{\mu_{SLR}}{\beta} \quad (8)$$

$$\sigma_{\ln(T)} = \frac{\sigma_{SLR}}{\beta} \quad (9)$$

where T_{ref} is the reference ARI, e.g., 100 years. Instead of the ARI, we use the frequency, $f = 1/T$, as the flood-hazard metric; that is, the projected annual frequency of flood depths exceeding the baseline 100-yr depth. In summary, except for the truncation issues to be addressed below, we have for flood depth a normal PDF with mean μ_d and standard deviation σ_{SLR} and for frequency a log-normal PDF with location parameter $\mu_{ln(T)}$ and scale parameter $\sigma_{ln(T)}$. The log normality of the flood frequency is consistent with the exponential increase in frequency with SLR described by Taherkhani et al (2020).

5.3 PDF Truncations and Mean Values

The depth and frequency PDFs need to be truncated because certain depths are prohibited. First of all, flood depth above ground cannot be negative. In addition, and more restrictive, depths at a location cannot be less than the MET required to reach the location from the coast. As described above, our modified bathtub analysis accommodates

https://doi.org/10.5194/egusphere-2023-425
Preprint. Discussion started: 18 April 2023

topographical flood barriers. Even where the storm-tide exceeds a location's elevation, if there is no path from the coast to the location along which the elevation is always lower than the storm tide, then no flooding occurs at the location. However, if the storm tide exceeds the MET, then the location floods to the full depth of storm tide minus elevation. This is illustrated in a one-dimensional fashion in Fig 9.

To prohibit flood depth between zero and $h_{MET} - h_{EL}$, where h_{MET} is the MET and h_{EL} the elevation above local mean sea level, we truncate the depth PDF at values below a truncation depth $d_{trnc} = h_{MET} - h_{EL}$. The probability removed is reassigned to a delta function at $d=0$. The frequency PDF must be truncated correspondingly. To determine the truncation frequency, we equate the standardized value of ln(T) to the standardized truncation depth. That is,

$$\frac{\ln(T)-\mu_{\ln(T)}}{\sigma_{\ln(T)}} = -\frac{d_{trnc}-\mu_d}{\sigma_{SLR}}. \quad (10)$$

The negative sign on the right-hand side of (10) is due to the fact that as depth increases (upward in Fig 8), $\ln(T)$ decreases (leftward in Fig 8). Substituting (8) and (9) into (10), using $\ln(f) = -\ln(T)$, and solving for f yields the truncation threshold frequency

$$f_{trnc} = f_{ref}\, e^{-(h_{ST}-h_{MET})/\beta} \quad (11)$$

where f_{ref} is the reference baseline frequency $f_{ref} = 1/T_{ref}$, e.g., $f_{ref} = 0.01$ yr^{-1}, the 100-yr reference ARI. For $f < f_{trnc}$, the probability in the log-normal frequency PDF is set to zero. The truncated probability is reassigned to a delta function at f_{ref}. In other words, disallowed frequencies associated with disallowed flood depths are assigned to the reference frequency; that is, the 100-yr baseline and projected flood depths are allowed to be zero.

Note that (11) is independent of SLR. The truncations for depth and frequency only depend on the elevation field and the baseline storm tide. The exponent in (11) can have either sign. For example, consider $d_{100} = 1.0$m, $h_{MET} = 0.5$m, and a typical GTSR value $b = 0.3$m. In this case, $f_{trnc} = 0.0019$yr^{-1}, and the truncation will have negligible impact on the moments of the PDF. By contrast, for $d_{100} = 1.0$m, $h_{MET} = 2.0$m and the same β, we have $f_{trnc} = 0.28$yr^{-1}, and the majority of the PDF probability is truncated and reassigned to 0.01yr^{-1}. Physically, in this second example the mean of the SLR distribution is not nearly high enough for the location to flood, and the most possible flood frequencies remain the baseline frequency. However, there is a small probability that SLR will be high enough (the right tail of the SLR distribution), in which case flooding becomes very frequent. Examples for both cases of depth and frequency PDFs are shown in Figs 10 and 11.

In summary, the depth and frequency PDFs, including truncations, are

https://doi.org/10.5194/egusphere-2023-425
Preprint. Discussion started: 18 April 2023

$$p(d) = \begin{cases} \frac{1}{\sigma_{\mathrm{SLR}}}\,\phi\,(\alpha_d^2), & d \geq d_{trnc} \\ \Phi(\alpha_d)\,\delta(d), & d < d_{trnc} \end{cases} \tag{12}$$

$$p(f) = \begin{cases} \frac{1}{f\sigma_{ln(T)}}\,\phi\,(\alpha_f^2), & f > f_{trnc} \\ \Phi(\alpha_f)\,\delta(f - f_{ref}), & f \leq f_{trnc} \end{cases} \tag{13}$$

where $\phi(x) = \frac{1}{\sqrt{2\pi}}\exp\left(-\frac{1}{2}x^2\right)$, $\Phi(x) = \frac{1}{2}\left(1+\mathrm{erf}\left(\frac{x}{\sqrt{2}}\right)\right)$, $\alpha_d = (d_{trnc} - \mu_d)/\sigma_{SLR}, \alpha_f = (\ln(f_{trnc}) + \mu_{ln(T)})/\sigma_{ln(T)}$, and $\delta(x)$ is the Dirac delta function. (Note that in the definition of α_f, the term $\mu_{ln(T)}$ enters with positive sign, due to the conversion from ARI to frequency, for which $\ln(f) = -\ln(T)$.)

The expectation, or mean, of the truncated depth PDF is

$$E_{d,trnc} = (1 - F)E(d|d > d_{trnc}) + F\,d_{zero} \tag{14}$$

where F is the truncated PDF probability fraction reassigned to flood depth $d_{zero} = 0$, and $E(d|d>d_{trnc})$ is the conditional expectation above d_{trnc}. This can be expressed as

$$E_{d,trnc} = (1 - \Phi(\alpha_d))\,\mu_d + \sigma_{SLR}\,\phi(\alpha_d)\,. \tag{15}$$

For frequency, the expectation of the truncated PDF is

$$E_{f,trnc} = f_{ref}\Phi(\alpha_f) + E_{f,uc}\Phi(\sigma - \alpha_f) \tag{16}$$

where $E_{f,uc} = \exp\left(\mu_{ln(T)} + \frac{1}{2}\sigma^2_{ln(T)}\right)$ is the "unconditional" log-normal PDF mean (the mean frequency without truncation considerations). Substituting (8) and (9) yields this unconditional mean frequency in terms of the SLR mean and standard deviation and the Gumbel scale parameter:

$$E_{f,uc} = \exp\left(\frac{\mu_{SLR}}{\beta} + \frac{\sigma^2_{SLR}}{2\beta^2}\right) \tag{17}$$

The unconditional mean frequency is independent of elevation, depending only on storm tide and SLR. As discussed below, there is a large range of elevations where the frequency approximates its unconditional mean value well.

Examples of flood-depth and frequency PDF projections and means are shown in Figs 10 and 11 for selected locations in coastal North Carolina. For the location in Fig. 10, the flood-depth and frequency truncations are negligibly small, and the PDFs display no visible truncations at any projected decade. By contrast, the location in Fig. 11 has intervening elevated topography between it and the nearby coast. This causes a significant truncation in the flood-depth and

https://doi.org/10.5194/egusphere-2023-425
Preprint. Discussion started: 18 April 2023

frequency PDFs. As indicated above, truncations are independent of SLR, and thus do not vary by decade. In addition to the mean flood-depth and frequency, the figures show the evolution in 90th, 95th, and 99th percentile values derived from the PDFs. For the truncated location of Fig 11, these high percentile values only exceed the baseline in late decades, when the tail of the SLR distribution is long enough to exceed the truncation.

5.4 Depth and Frequency Sensitivity to Elevation

The expressions (15) and (16) for mean flood depth and frequency have different sensitivities to ground elevation, as illustrated in Fig 12 for typical parameter values. In the case of no intervening elevation barrier between the coastal storm-tide and a location of interest (red curves in Fig. 12), the flood depth declines approximately linearly with elevation, until a tail region of low flood depth and slower decline is reached above about 1.5m elevation. Meanwhile, the frequency is approximately constant between roughly 0 and 1.5m of elevation and 0 and 1.5m of flood depth. In this regime, $E_{f,trnc} \sim E_{f,uc}$, approximately 10yr^{-1} for these parameter values. The truncated probability in the frequency PDF is negligible, and the mean frequency is simply determined by the storm tide and SLR characteristics, independent of elevation. At higher elevation, the frequency truncation becomes impactful, and the mean frequency declines, ultimately limiting to the reference value. In this truncation regime, frequency declines more slowly than flood depth, due to the longer tail of the log-normal PDF. At such elevations, frequency can be well elevated above the baseline value, even though flood depth is near zero, as seen in the right panel of Fig. 12. For the case of intervening elevation barriers (light and dark blue curves in Fig 12), the frequency truncation is impactful at all elevations.

It may seem counterintuitive that there is a regime where projected flood frequency does not depend on ground elevation and is uncorrelated with flood depth. This is a straightforward consequence, however, of the fact that both the historical baseline and projected flood depths vary with elevation. The flood frequency metric diagnoses change of projected depth with respect to the baseline, and in this regime the baseline and projected depths have the same elevation dependence. The only remaining factors to affect frequency change are the coastal storm tide characteristics and SLR. As discussed below, the insensitivity of the frequency hazard metric to elevation has advantages and disadvantages.

6 Flood Map Examples

Examples of mean projected flood depth and frequency are shown in Figs 13 through 16 for a 6-km region of coastal North Carolina near North Topsail Beach using both the higher-resolution 3DEP DEM (1-arc-second) and the lower-resolution MERIT DEM (3-arc-second). Much of the North Topsail Beach region is subject to coastal flooding, increasingly so in later decades. In the 3DEP-based analysis, maximum flood-depth values in the 2090s under the high-emissions RCP8.5 climate scenario are 1.9m for the 10-yr ARI, 2.5m for the 100-yr ARI, and 3.7m for the 1000-yr ARI event, compared to 1.2m, 1.7m, and 2.9m for the baseline. In the MERIT-based analysis, the corresponding 2090s projected values are lower: 1.2m for 10-yr, 1.8m for 100-yr, and 3.0m for 1000-yr ARIs, compared to 0.4m,

https://doi.org/10.5194/egusphere-2023-425
Preprint. Discussion started: 18 April 2023

1.0m, and 2.2m for the baseline. The 3DEP-MERIT discrepancies, driven by elevation differences, are typical of low-lying unbuilt environments, and the discrepancies can be considerably larger in urban environments. Another difference is that MERIT and 3DEP mark elevation of the tidal bays behind open-ocean beach differently (e.g., Alligator Bay in the center of Figs 13 and 15), with MERIT indicating non-zero elevation and 3DEP providing an open-water flag. Consequently, our depth-frequency analysis computes flood values on the MERIT bays, but not on the 3DEP bays.

For both the 3DEP- and MERIT-based Topsail-Beach analysis there is more spatial variability in projected flood depth (Figs 13 and 15) than there is in the projected frequency (Figs. 14 and 16). (Note that we only calculate and plot the frequency if the 2090s 1000-yr flood depth at the 99th percentile is non-zero.) As illustrated in Fig. 12, mean flood depth is directly sensitive to elevation, while frequency is insensitive in the low-elevation regime. In the low-elevation regime, frequency depends only on characteristics of the coastal storm tide and SLR, which vary more smoothly than elevation. In fact, the 2090s maximum projected frequency for this coastal North Carolina region is the same for the 3DEP and MERIT-based analyses: 0.18yr^{-1}. The independence of frequency on elevation data can be seen graphically in Fig. 17. Scatter plots across the region of 2090s frequency vs elevation depth are nearly identical for 3DEP and MERIT. The shape shown in Fig. 12 (center) is reflected in both: a regime of elevation-independent frequency followed by a decline with elevation.

An additional example is shown in Fig. 18 for the Miami Beach, Florida area. Most of the region is subject to coastal flooding. The 100-yr mean flood-depth field in the 2090s varies spatially, from near zero to close to 2m in the high emissions RCP8.5 scenario. Meanwhile, the 2090s frequency of the baseline 100-yr flood depth is an almost uniform 0.3 yr^{-1}, approximately 30 times the baseline frequency. Most of the area is in the regime where the frequency is approximates its unconditional value, determined only by storm tide and SLR. In only a few small regions is elevation high enough to sit outside the unconditional regime, and truncations due to elevation reduce the frequency.

Projected evolution of the mean flood depth and frequency of the baseline 100-yr event are shown in Fig 19 for Miami Beach City Hall. The mean 100-yr flood depth increases steadily from 0.05m to 0.75m, while the annual frequency increase is closer to exponentially, from the 0.01 yr^{-1} baseline to about 0.3 yr^{-1} in the 2090s. Also shown in the figure are depth and frequency 90th, 95th, and 99th percentiles, derived from the PDFs. The 99th percentile flood depth reaches about 1.25m in the 2090s, while the 99th percentile annual frequency of the baseline 100-yr event exceeds 2.0 yr^{-1}.

7 Conclusions

We have presented efficient methodology to summarize the hazard of coastal flooding with sea-level rise. The distribution of flood depth above ground is determined using coastal storm-tide levels at a range of ARIs (Muis et al, 2016), SLR projections (Kopp et al., 2014), and a flood-water path-finding algorithms applied to DEMs. These are approximate flood-depth estimates, as no account is taken of key influential factors, such as waves, flood-water

https://doi.org/10.5194/egusphere-2023-425
Preprint. Discussion started: 18 April 2023

propagation rates, and meteorological event details. However, we have shown that in the Gumbel extreme-value limit of storm tide analysis, when the projected ARI of the historical baseline 100-yr flood depth is considered, the results are more robust, approximately independent of many of these detailed factors. In addition, the map of projected ARIs has less sensitivity to DEM uncertainties than does flood depth. We also show that, in the Gumbel limit, calculation of the fractional change in structure loss from flood under SLR can be performed at a single ARI, e.g., 100 years, and then applied to any other ARI or to a change in loss averaged over all ARIs. Computational savings are realized by avoiding detailed event-based meteorological and hydraulic modeling, savings which are essential when climate risks need to be modeled and projected rapidly to multiple perils and decades at large numbers of global locations.

The relative insensitivity of the ARI hazard metric to ground elevation has advantages and disadvantages. DEMs have considerable uncertainty (e.g., Hawker et al., 2018), and currently available global DEMs may not be sufficiently accurate to estimate flood levels driven by SLR of less than one meter (Gesch, 2018). Thus, relative insensitivity to such uncertainty is advantageous. On the other hand, flood depth has direct physical connection to structure damage, while the impact of increased flood frequency is less direct. The increased frequency of a negligible flood depth may not be material for damage and loss. Detailed high-resolution flood modeling is essential for estimating damage and loss to buildings and infrastructure, and ARI analysis is not a substitute for such modeling. However, as a computationally efficient first-pass analysis that can be applied on a global scale with reduced sensitivity to DEM uncertainties, it has significant utility.

https://doi.org/10.5194/egusphere-2023-425
Preprint. Discussion started: 18 April 2023

Appendix: Timescale Relationships and the Gumbel distribution

The Gumbel distribution, often used to model the distribution of maximum values of a random variable in a series of specified time intervals, is derived from a Poisson process for the event occurrence, for example storm tide with water level above a specified threshold in a year. For Poisson processes, the distribution of intervals between events is exponential. That is, the probability of waiting longer than time interval t between events is

$$P(T > \tau) = e^{-f\tau} \quad \text{(A1)}$$

where f is the event frequency, the average number of events per τ.

The average recurrence interval (ARI) is $T_{ARI} = 1/f$. The ARI is distinct from the return period (RP), which is the reciprocal of the probability of an event in interval t; i.e., $T_{RP} = t/P(T<\tau)$. T_{ARI} is the average time between successive events, while T_{RP} is the average time to wait for the next interval τ with at least one event. In the large ARI or RP limit $T_{ARI} \sim T_{RP}$, but for smaller RPs they differ. For example, T_{RP} is always greater than τ, while T_{ARI} can take any positive value. From equation (A1), the probability of waiting *less* than interval τ between events, $1-P(T>\tau)$, is

$$P(T < \tau) = 1 - e^{-f\tau} \quad \text{(A2)}$$

We are interested in $\tau = 1$ year. Therefore $P(T<1) = 1-e^{-f}$ is the probability that at least one event happens in a year, and $T_{RP} = 1/P(T<1)$. Therefore, we have the relationship between T_{RP} and T_{ARI}

$$T_{RP} = \frac{1}{1-\exp\left(-\frac{1}{T_{ARI}}\right)}, \quad \text{(A4)}$$

where the numerator on the right of (A4) has units of time, i.e., 1 year. Equation (A4) is sometimes referred to as Longbein's formula (Longbein, 1949), and relevant discussion can be found in Ball et al (2019). Note that (A4) confirms that in the large RP limit, $T_{ARI} \sim T_{RP}$.

Now consider the Gumbel distribution for the maximum events per year. The Gumbel CDF at x (the probability of annual maximum x' less than x) is

$$P(x' < x) = e^{-e^{-(x-\mu)/\beta}} \quad \text{(A5)}$$

where μ and β are the location and scale parmeters. The probability that x' exceeds x is $1-P(x'<x)$, and therefore the RP is $T_{RP} = 1/(1-P(x'<x))$. Substituting equation (A4) for T_{RP} and solving for x yields

https://doi.org/10.5194/egusphere-2023-425
Preprint. Discussion started: 18 April 2023

$$x = \beta \ln(T_{ARI}) + \mu \quad \text{(A6)}$$

Therefore, x is a log-linear function of the ARI, the average time interval between successive occurrences of and event with magnitude x.

If instead of the Gumbel we consider GEV with non-zero shape parameter ξ, then $P(x'<x)$ in (A5) generalizes to $P(x' < x) = \exp(-t(x))$, where $t(x) = (1 + \xi\alpha)^{-1/\xi}$, and $\alpha = (x - \mu)/\beta$. (P(x'<x) equals (A5) for $\xi = 0$.) The relationship between x and T_{ARI} is then

$$x = \beta \left(\frac{T_{ARI}^{\xi} - 1}{\xi}\right) + \mu. \quad \text{(A7)}$$

Note the limiting behavior: $\lim_{\xi \to 0} \left(\frac{T_{ARI}^{\xi} - 1}{\xi}\right) = \ln(T_{ARI})$.

https://doi.org/10.5194/egusphere-2023-425
Preprint. Discussion started: 18 April 2023

Data Availability

The data used in this analysis are publicly available. Links to the sea-level rise data are found in Kopp et al (2014). Links to the GTSR storm-tide data are found in Muis et al (2016). The USGS 3DEP DEM data can be downloaded from https://www.sciencebase.gov/catalog/item/4f70aa71e4b058caae3f8de1. The MERIT DEM data can be downloaded from http://hydro.iis.u-tokyo.ac.jp/~yamadai/MERIT_DEM/index.html. The tropical cyclone data can be downloaded from https://www.ncei.noaa.gov/products/international-best-track-archive.

Author Contribution

TH, JK, and TT developed the study. TH performed analysis, produced the figures, and prepared the manuscript, with contributions from SB in diagnosing outputs and completing quality assurance. KD and DM participated in development and application discussions. All authors edited the manuscript.

Competing Interests

The authors declare that they have no conflicts of interest.

Acknowledgements

The authors acknowledge the support of The Climate Service, and S&P Global company.

https://doi.org/10.5194/egusphere-2023-425
Preprint. Discussion started: 18 April 2023

595 **References**

Ball, J., et al., editors: Australian Rainfall and Runoff: A Guide to Flood Estimation, Commonwealth if Australia (Geoscience Australia), book.arr.org.au.s3-website-ap-southeast-2.amazon.com, 2019.

Bates, P. D., et al.: Combined modeling of US fluvial, pluvial, and coastal flood hazard under current and future
600 climates, Water Res. Research, 57, e2020WR028673, doi:10.1029/2020WR028673, 2021.

Gesch, D. B.: Best practices for elevation-based assessments of sea-level rise and coastal flooding exposure, Front. Earth Sci., 12, doi.org/10.3389/deart.2018.00230, 2018.

Grady, C. J. and L. Xingong: A distributed approach for calculating inundation height based on Dijkstra's algorithm, Transactions in GIS, 22, 737-759, doi:10.1111/tgis.12453, 2018.

605 Hawker, L., et al.: Perspectives on digital elevation model (DEM) simulation for flood modeling in the absence of a high-quality open access global DEM, Front. Earth Sci., doi:10.3389/feart.2018.00233, 2018.

Hunter, J.: A simple technique for estimating an allowance for uncertain sea-level rise, Climatic Change, 113, 239-252, doi:10.1007/s10584-011-0322-1, 2012.

Kirezci, E., et al.: Projections of global-scale extreme sea levels and resulting episodic coastal flooding over the 21st
610 century, Nature Sci. Rep., 10.11629, doi.org/10.1038/s41598-020-67736-6, 2020.

Kopp, R. E., et al.: Probabilistic 21st and 22nd century sea-level projections at a global network of tide-gauge sites, Earth's Future, doi:10.1002/2014EF000239, 2014.

Levinson, D. H., et al.: Toward a homogeneous global tropical cyclone best track dataset, Bull Amer. Meteor. Soc., 91, 377-380, doi:10.1175/2010MABS2930.1, 2010.

615 Lin, N. et al.: Hurricane Sandy's flood frequency increasing from 1800 to 2100, Proc. Natl. Acad. Sci, 113, 12071-12075, doi:10.1073/pnas.1604386113, 2016.

Longbein, W. B.: Annual floods and the partial-duration flood series, Trans. Amer. Geophys. Union, 30, 879-881, doi:10.1029/TR030i006p00879, 1949.

Marsooli, R., et al.: Climate change exacerbates hurricane flood hazards along US Atlantic and Gulf Coasts in spatially
620 varying patterns, Nature Comm, doi:10.1038/s41467-019-11755-z, 2019.

McClean, F., Dawson, R., and Kilsby, C.: Implications of using global digital elevation models for flood risk analysis in cities, Water Resources Research, 56, e2020WR028241, doi:10.1029/2020WR028241, 2020.

Muis, S., et al.: A global reanalysis of storm surge and extreme sea levels, Nature Comm., doi: 10.1038/ncomms11969, 2016.

625 Muis S., et al.: A high-resolution global dataset of extreme sea levels, tides, and storm surges, including future projections, Frontiers Marine Sci., 7, 263, doi:10.3389/fmars.2020.00263, 2020.

Papalexiou, S. M., and D. Koutsoyiannis: Battle of the extrema value distributions: A global survey on extreme daily rainfall, Water Res. Research, 49, 187-201, doi:10.1029/2012WR012557, 2013.

Sayre, R., et al.: A new 30-meter resolution global shoreline vector and associated global islands database for the
630 development of standardized ecological coastal units, J. Operational Oceanography, 12, S47-S56, doi:10.1080/1755876X.2018.1529714, 2019.

https://doi.org/10.5194/egusphere-2023-425
Preprint. Discussion started: 18 April 2023

Scawthorn, C., et al.: HAZUS-MH flood loss estimation methodology. II. Damage and loss assessment, Nat. Hazards Rev., 7, 72-81, doi:10.1061/(ASCE)1527-6988(2006)7:2(39), 2006.

Stoker, J. M., and B. Miller: The accuracy and consistency of 3D elevation program data: A systematic analysis, Remote Sensing, 14, 940-964, doi:10.3390/rs1400940, 2022.

Sweet, W. V., et al.: Global and Regional Sea Level Rise Scenarios for the United States: Updated Mean Projections and Extreme Water Level Probabilities Along U.S. Coastlines, NOAA Tech. Rep. NOS 01, NOAA, Silver Spring MD, 2022.

Taherkhani, M., et al.: Sea-level rise exponentially increases coastal flood frequency, Nature Sci. Rep., 10:6466, doi:10.1038/s41598-020-62188-4, 2020.

Vitousek, S., et al.: Doubling of coastal flooding frequency within decades due to sea-level rise, Nature Sci. Rep., 7, 1399, doi:10.1038/s41598-017-01362-7, 2017.

Vousdoukas, M. I., et al.: Global probabilistic projections of extreme sea levels show intensification of coastal flood hazard, Nature Comm., 9:2360, doi:10.1038/s41467-018-04692-w, 2018.

Wahl, T., et al: Understanding extreme sea levels for broad-scale coastal impact and adaptation analysis, Nature Comm., 8:16075, doi: 10.1038/ncomms16075, 2017.

Wing, O. E. J., et al.: New insights into US flood vulnerability revealed from flood insurance big data. Nature Comm., 11:1444, doi:10.1038/s41467-020-15264-2, 2020.

Yamazaki, D., et al.: A high-accuracy map of global terrain elevations, Geophys. Res. Lett., 44, 5844-5853, doi:10.1002/2017GL072874, 2017.

Zervas, C.: Extreme water levels of the United States 1893-2010, NOAA Tech Report NOS CO-OPS 067, 2013.

https://doi.org/10.5194/egusphere-2023-425
Preprint. Discussion started: 18 April 2023

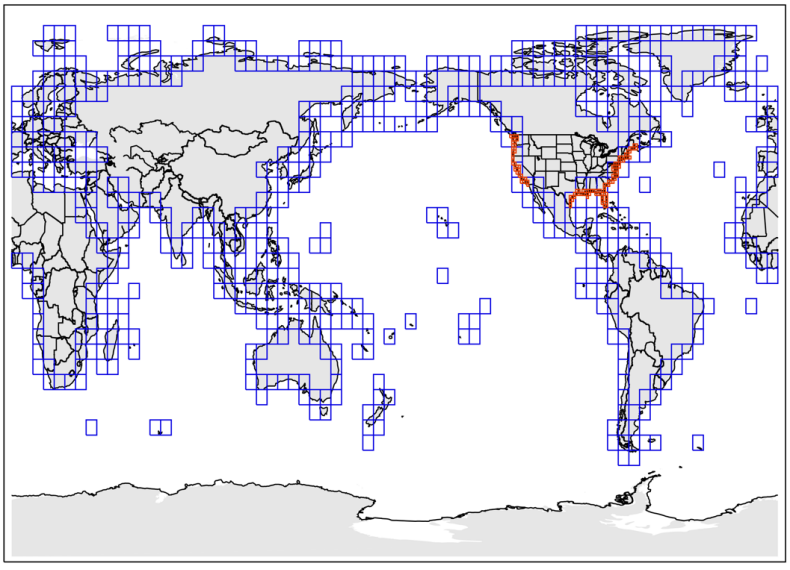

Figure 1: Map of the domain tiles. Blue: MERIT-based 5°-by-5° tiles. Red: 3DEP-based 1°-by-1° tiles.

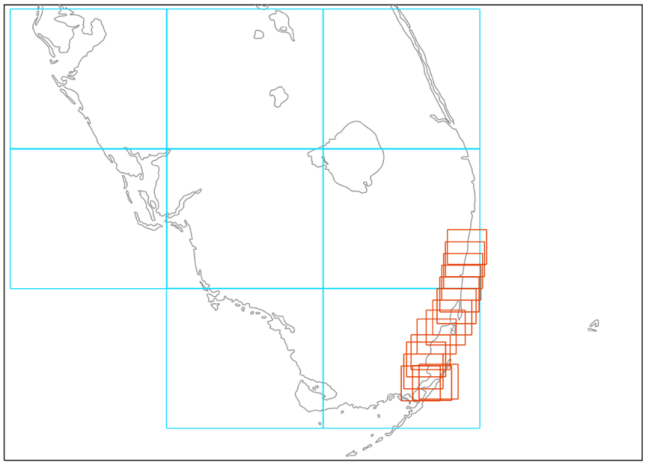

Figure 2: Examples of DEM tiles and MET boxes along southeast Florida. The blue rectangles indicate 1°-by-1° 2DEP DEM tiles and the red boxes indicates 0.25°-by-0.25° MET calculation boxes, with centers spaced along the USGS-defined coastline by 12.5km.

https://doi.org/10.5194/egusphere-2023-425
Preprint. Discussion started: 18 April 2023

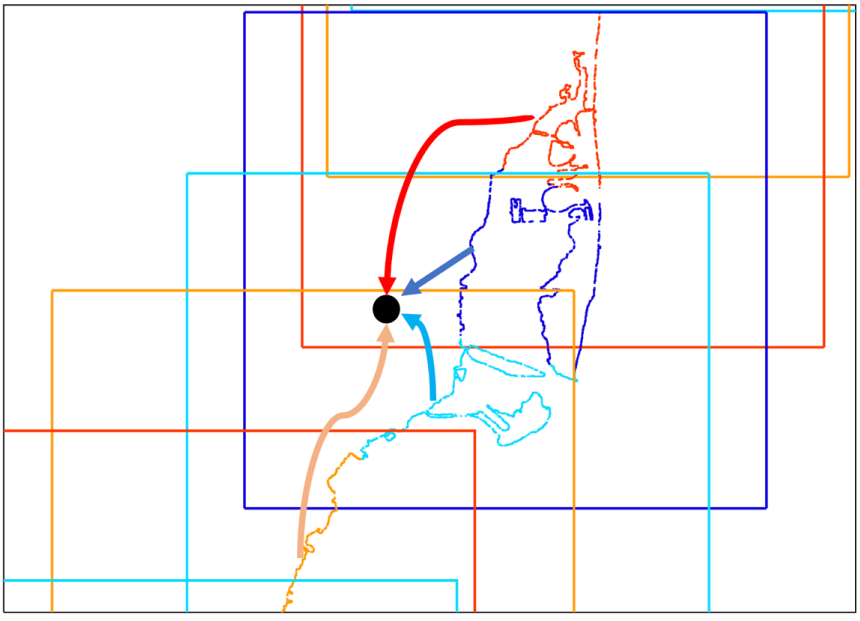

Figure 3: Illustration of multiple paths and METs. An interior location of interest is indicated by the black symbol. The location sits inside four MET boxes, colored red, orange, light blue, and dark blue. The USGS-defined coastal pixel sets associated with each box that are closer to that box's center than any other box center are indicated by the small colored points along the coast. Colored arrows represent four possible distinct paths to the interior location from each set of coastal pixels.

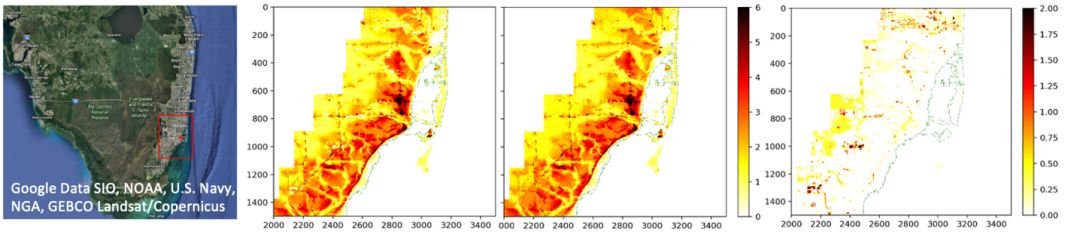

Figure 4: Examples of elevation and MET maps and their difference. The Miami region of southeast Florida is selected for illustration, as indicated by the red rectangle in the left panel. The USGS 3DEP elevation map is shown second from left, color-contoured in meters on the 0-to-6m scale. Third from left is the calculated MET map. The rightmost panel is MET minus the elevation on the 0-to-2m scale.

https://doi.org/10.5194/egusphere-2023-425
Preprint. Discussion started: 18 April 2023

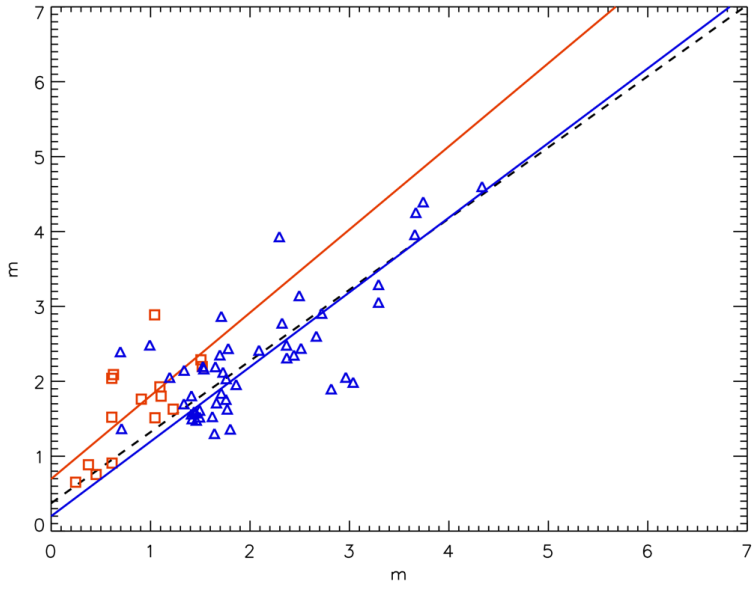

675 **Figure 5: Scatter plots of 100-year storm-tide estimates from 82 NOAA tide-gauge stations (Zervas, 2013) on the y axis and GTSR values (Muis et al., 2016) at the same locations on the x axis. Locations in active TC regions (south of 30°N and east of 100°W) and shown in red, and symbols outside the TC region are shown blue. The black dashed line is the OLS linear fit through all the locations. The red and blue lines are fits using only locations from the TC and non-TC regions, respectively.**

680

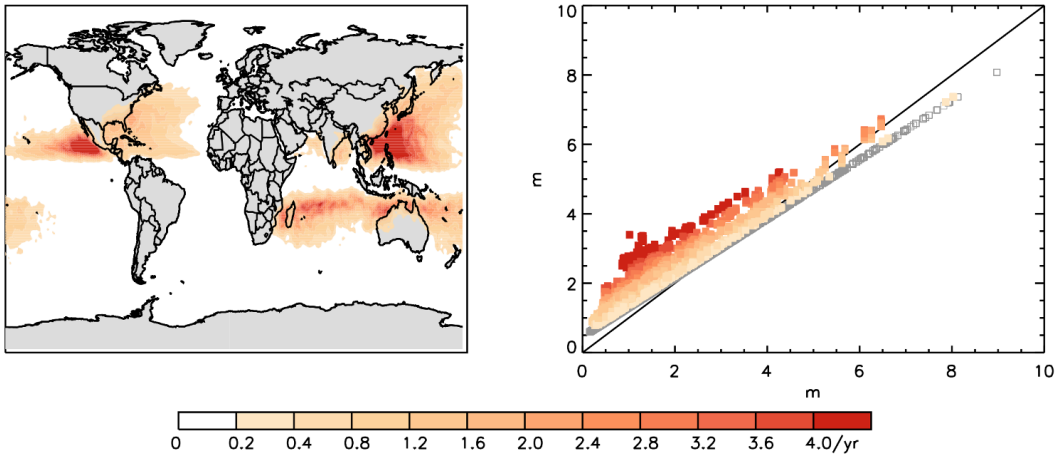

Figure 6: Left: Gridded smoothed TC annual occurrence rate (tropical storm force and greater) computed from IBTrACS and used in the storm-tide debiasing procedure. Right: Scatter plot across a set of global locations of the debiased 100-year ARI storm tide (y axis) vs the raw GTSR values (x axis). Symbols are color

https://doi.org/10.5194/egusphere-2023-425
Preprint. Discussion started: 18 April 2023

685 **coded by the TC annual occurrence rates in the right panel using the same color scale, with white regions (left) and unfilled symbols (right) indicating levels below 0.2 yr^{-1}.**

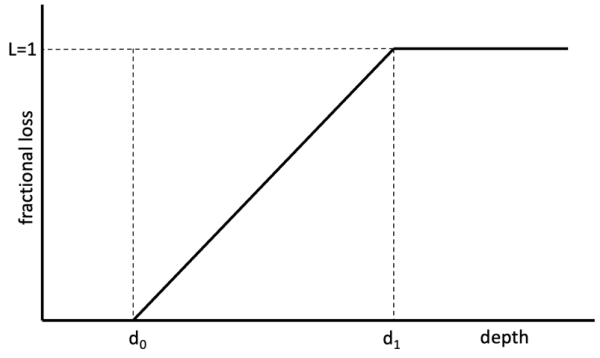

Figure 7: Illustration of a simple fractional form for fractional loss to a structure as a function of flood depth at the structure.

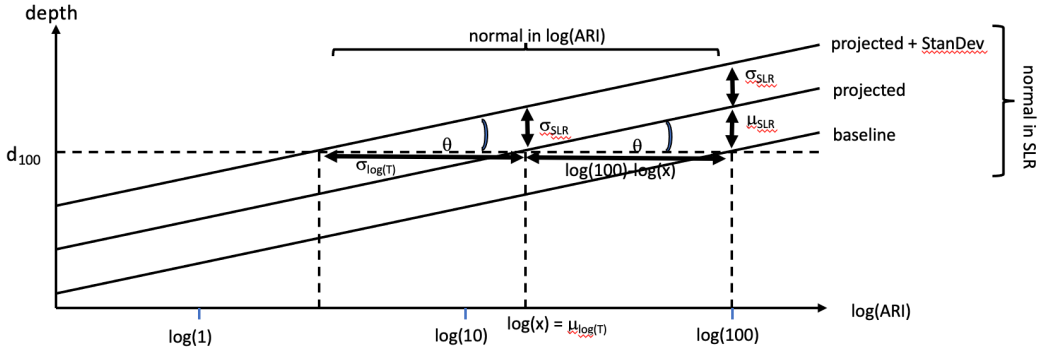

690

Figure 8: Illustration of the relationship between flood depth (vertical axis) and log ARI (horizontal axis). The bottom sloping curve represents the baseline log-linear depth-ARI relationship. The depth where *T*=100yr, indicated by the right vertical dashed line, is the 100-yr flood depth, d_{100}, indicated by the horizontal dashed line. When mean projected SLR, μ_{SLR}, is added, the depth-ln(T) curve shifts upward to the middle curve. The 695 **top curve is an upward shift by one SLR standard deviation, σ_{SLR}, above the mean. See discussion for further details.**

https://doi.org/10.5194/egusphere-2023-425
Preprint. Discussion started: 18 April 2023

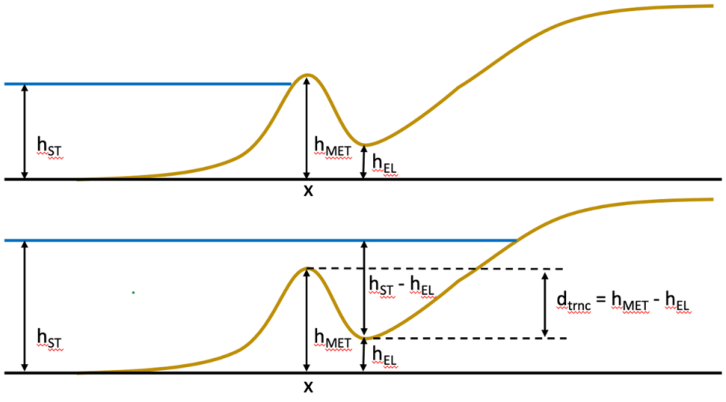

Figure 9: One-dimensional illustration of 100-yr storm tide, elevation, and MET. The black line indicates local sea level, the brown curve indicates ground elevation moving inland from left to right, and the blue line indicates storm-tide level. In the top panel, although the storm tide level h_{ST} is greater than the elevation h_{EL} at location x, the intervening barrier of elevation h_{MET} prevent x from being flooded. In the bottom panel, the storm tide is higher, and x is flooded to depth $h_{ST} - h_{EL}$. Note that it is not possible at x to have a flood depth less than $d_{trnc} = h_{MET} - h_{EL}$. Thus, the PDF of depths at x has probability density at zero depth and depth greater than $h_{MET} - h_{EL}$, but zero probability density in between.

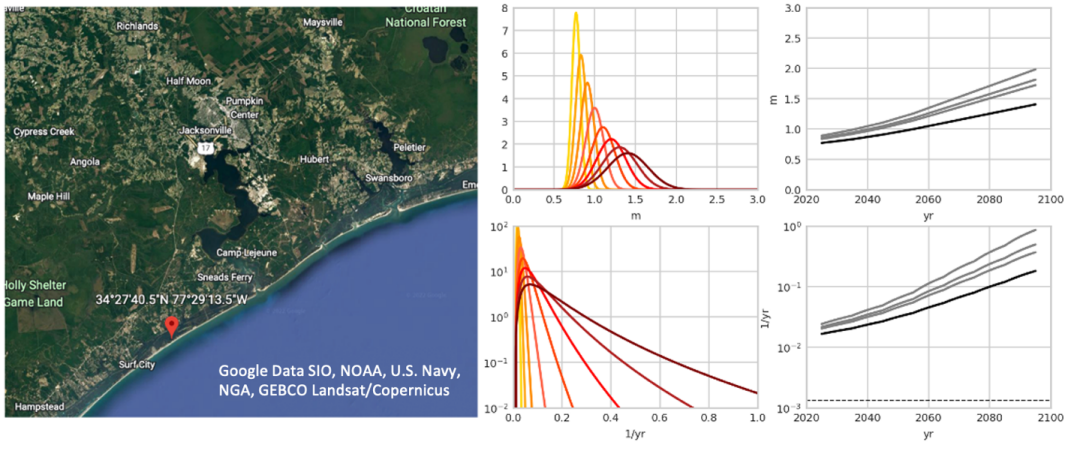

Figure 10: Example of flood depth and frequency analysis at 77.487083°W and 34.461250°N on coastal North Carolina with and elevation h_{EL} = 0.3m and MET h_{MET} = 0.3m based on the 3DEP DEM. The location is indicated by the red marker in the left panel. Flood-depth PDFs (top center) and frequency PDFs (bottom center) are shown by decade 2020s to 2090s yellow to dark red. Mean flood depth (top right) and mean frequency (bottom right) are shown black by decade and the 90th, 95th, and 99th percentiles values are shown gray. The depth-PDF truncation (minimum positive flood depth) is $h_{MET} - h_{EL}$ = 0, and the corresponding

https://doi.org/10.5194/egusphere-2023-425
Preprint. Discussion started: 18 April 2023

truncation frequency is 0.002yr^{-1}, indicated by the horizontal dashed line. The truncated flood-depth and frequency probabilities, reassigned to depth zero and baseline frequency 0.01yr^{-1}, respectively, are negligible in this example.

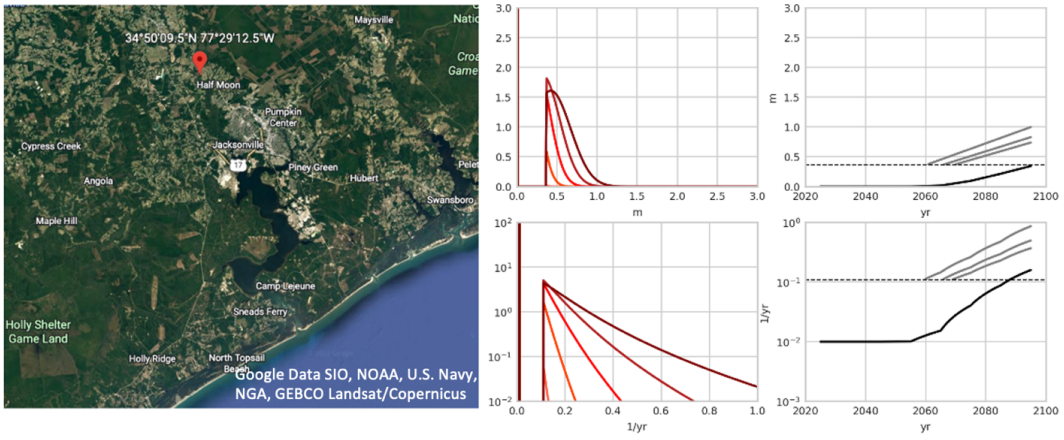

Figure 11: As in Fig 10, but for the inland location 77.486806°W 34.835972°N near the New River, with elevation h_{EL} = 1.3m and h_{MET} = 1.7m. The depth-PDF truncation is $h_{MET} - h_{EL}$ = 0.4m, corresponding to the minimum possible non-zero flood depth at the site. Intermediate topography between coastal points (here, along the Cape Fear River) and the location protect the location from flooding below this level. The corresponding frequency truncation is 0.11yr^{-1}. The truncations and reassigned probabilities are clearly visible in the PDFs. These depth and frequency truncations are indicated by dashed lines in the right panels. The mean flood depth and frequency, means over the PDFs, can have values below the truncations, as they are influenced by the delta functions. However, in this example, the 90th, 95th, and 99th percentiles only become greater than the 0.01yr^{-1} baseline when the PDF tails reach far enough beyond the truncations.

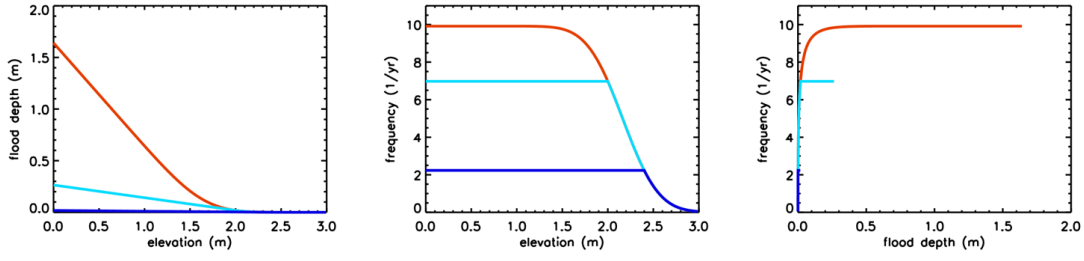

Figure 12: Mean flood-depth (left) and frequency (enter) as functions of elevation, h_{EL}, and frequency as a function of flood depth (right), as determined by equations (15) and (16). For these illustrations, the 100-yr storm-tide is 0.6m, mean SLR is 1.0m, SLR standard deviation is 0.3m, and the Gumbel scale parameter is b = 0.18m. Red shows the case of no intervening elevation barrier (h_{MET} = 0), light blue the case of a 2.0m intervening elevation barrier (h_{MET} = 1.0m if h_{EL} < 1.0m, and h_{MET} = h_{EL} otherwise), and dark blue the case of a 2.4m intervening barrier (h_{MET} = 2.4m if h_{EL} < 2.4m, and h_{MET} = h_{EL} otherwise).

https://doi.org/10.5194/egusphere-2023-425
Preprint. Discussion started: 18 April 2023

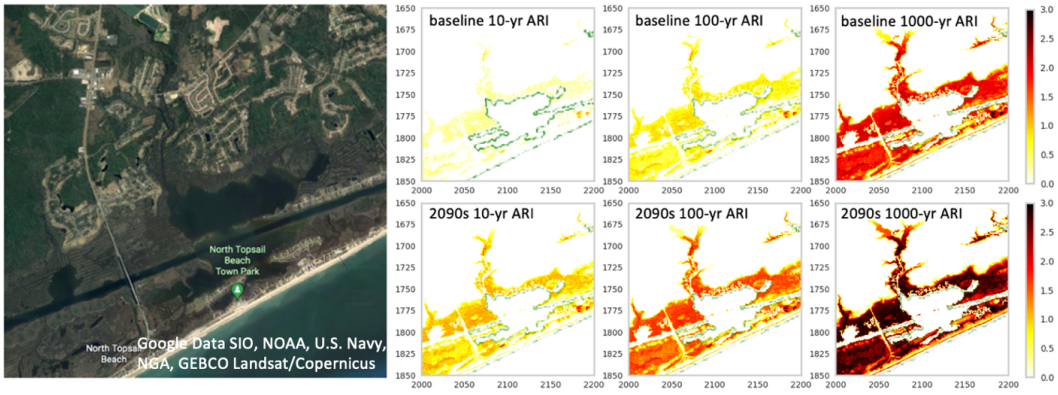

Figure 13: Coastal North Carolina in the North Topsail Beach region (left) and maps of baseline and projected mean flood depth in meters (right six panels). The top row shows the historical baseline 10-yr, 100-yr, and 1000-yr ARI flood depth, left to right. The bottom row is the projected 2090s RCP8.5 10-yr, 100-yr, and 1000-yr flood depth (left to right). Labels on the flood map axes are 1 arc-second (~30m) pixel counts, and the regions shown span 200 by 200 pixels, approximately 6km square. The USGS-defined continental coastline is shown in green.

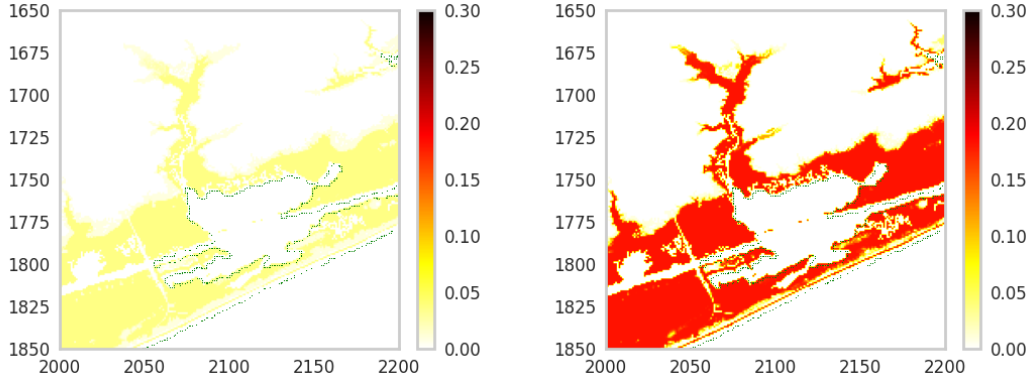

Figure 14: Projected RCP8.5 frequency (units yr^{-1}) for the 2050s (left) and 2090s (right) of the baseline 100-year flood depth for the same region as Fig 13. Note the reduced variability in frequency compared to flood depth, illustrating the reduced sensitivity of the frequency hazard variable to elevation.

https://doi.org/10.5194/egusphere-2023-425
Preprint. Discussion started: 18 April 2023

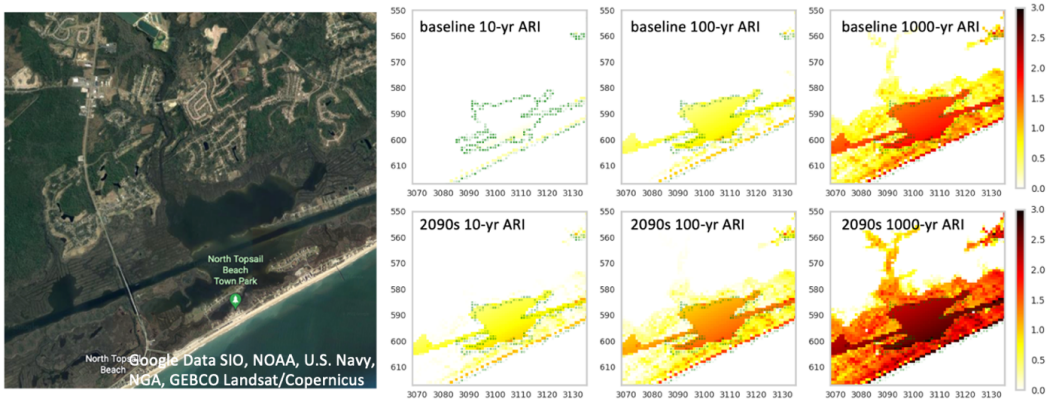

Figure 15: As in Fig 13, but here using the lower-resolution (3 arc-second) MERIT DEM. The x- and y-axis labels indicate MERIT pixel counts, 67 by 67 pixels covering the same coastal NC region.

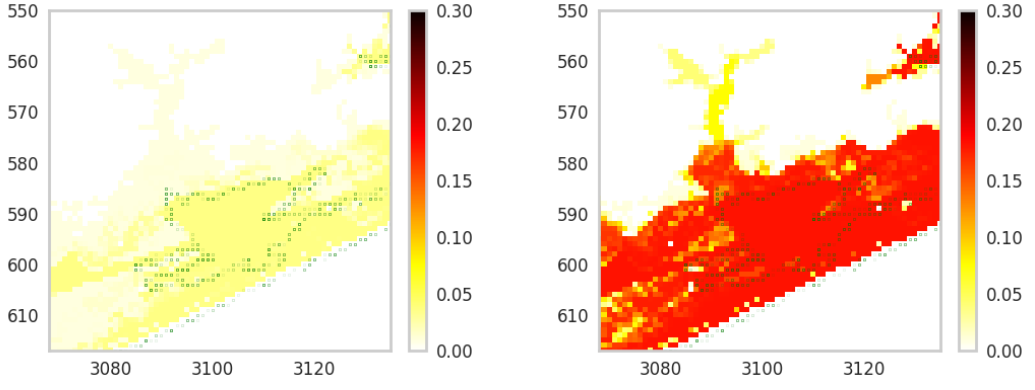

Figure 16: As in Fig 14, but here using the lower-resolution (3-arc-second) MERIT DEM. The x- and y-axis labels indicate MERIT pixel counts, 67 pixels covering the same coastal NC region.

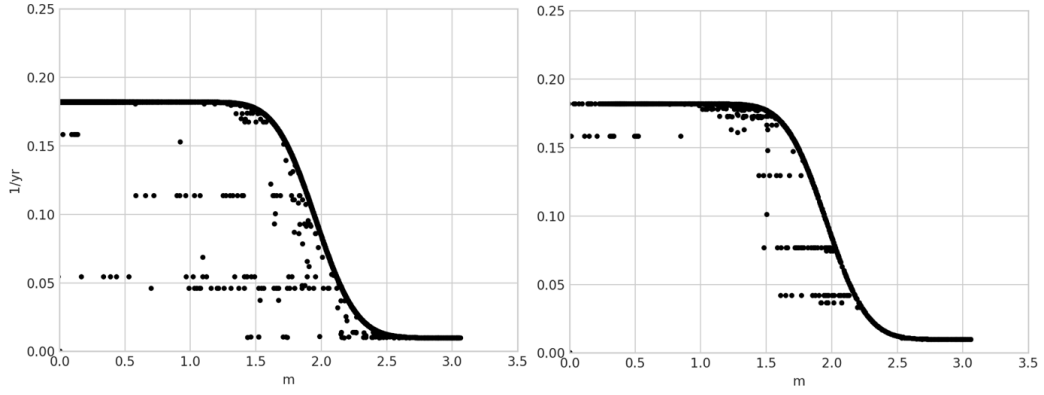

Figure 17: Scatter plots of RCP8.5 2090s projected frequency vs elevation across the spatial domains of Figs. 13 and 14. Left: the 3DEP DEM (Figs. 13 and 14). Right: the MERIT DEM (Figs 15 and 16).

https://doi.org/10.5194/egusphere-2023-425
Preprint. Discussion started: 18 April 2023

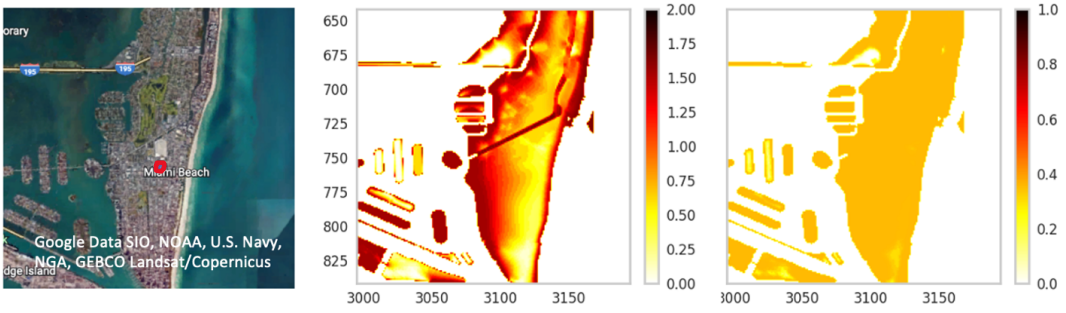

Figure 18: Miami Beach , Florida RCP8.5 2090s. Left: map of region. Center: projected mean 100-yr RP flood-depth (m). Right: projected mean frequency (yr^{-1}) of baseline 100-yr depth. Notice that projected flood-depth varies spatially, while frequency is almost uniform. This region is in a regime where frequency is approximately independent of elevation, as discussed in Section 5.4. The red circle in the left panel indicates the location of Miami Beach City Hall for Fig. 19.

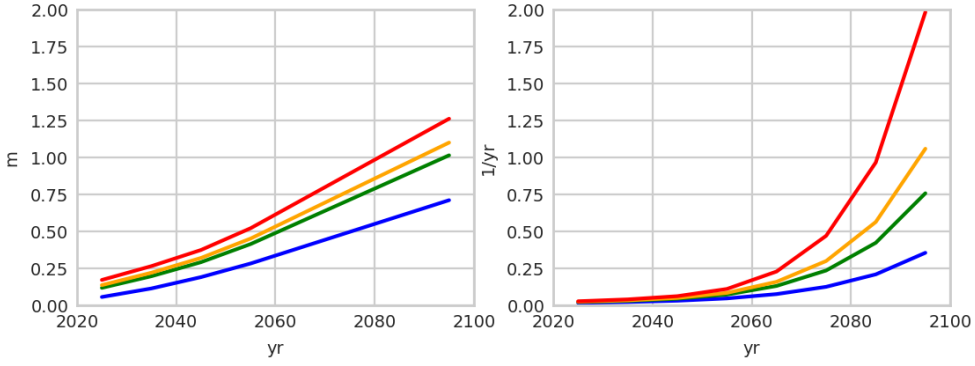

Figure 19: Projected evolution in flood depths (left) and frequencies (right) at Miami Beach City Hall under scenario RCP8.5. (The location is indicated by the red circle in the left panel of Fig 18.) Left: 100-year mean flood-depth (blue) and flood-depth at three percentiles: 90th (green), 95th (orange), and 99th (red). Right: Mean projected frequency of the baseline 100-year flood depth and the frequency at the 90th, 95th, and 99th percentiles.